ADVANCED MATERIALS
www.advmat.de

Nanoparticle-Mediated Delivery of Anti-PU.1 siRNA via Localized Intracisternal Administration Reduces Neuroinflammation

William T. Ralvenius, Jason L. Andresen, Margaret M. Huston, Jay Penney, Julia Maeve Bonner, Owen S. Fenton, Robert Langer,* and Li-Huei Tsai**

Neuroinflammation is a hallmark of neurodegenerative disorders including Alzheimer's disease (AD). Microglia, the brain's immune cells, express many of the AD-risk loci identified in genome wide association studies and present a promising target for anti-inflammatory RNA therapeutics but are difficult to transfect with current methods. Here, several lipid nanoparticle (LNP) formulations are examined, and a lead candidate that supports efficient RNA delivery in cultures of human stem cell-derived microglia-like cells (iMGLs) and animal models of neuroinflammation is identified. The lead microglia LNP (MG-LNP) formulation shows minimal toxicity and improves delivery efficiency to inflammatory iMGLs, suggesting a preference for delivery into activated microglia. Intraperitoneal injection of the MG-LNP formulation generates widespread expression of the delivered reporter construct in all organs, whereas local intracisternal injection directly into the cerebrospinal fluid leads to preferential expression in the brain. It is shown that LNP-mediated delivery of siRNA targeting the PU.1 transcription factor, a known AD-risk locus, successfully reduces PU.1 levels in iMGLs and reduces neuroinflammation in mice injected with LPS and in CK-p25 mice that mimic the chronic neuroinflammation seen in AD patients. The LNP formulation represents an effective RNA delivery vehicle when applied intrathecally and can be broadly utilized to test potential neuroinflammation-directed gene therapies.

1. Introduction

Several neurodegenerative disorders, including Alzheimer's disease (AD), are characterized by a state of neuroinflammation.[1–3] As one of the most prevalent and deadly neurological diseases, AD has been subject to decades of research and clinical efforts in search of potential therapeutic remedies.[4,5] Although antibodies designed to clear β-amyloid have recently shown therapeutic potential in human patients, the multifaceted nature of AD suggests a need for diverse treatment approaches depending on disease pathology and progression.[6] Microglia, the major immune cells present in the brain, have been subject of increasing interest for their potential role in the onset or prevention of AD.[2,7,8] A majority of AD risk genes identified through genome wide association studies are highly expressed in microglia,[9] including the transcription factor PU.1, which is centrally involved in the regulation of basic microglia functions.[10] Several studies have shown that increased

W. T. Ralvenius, M. M. Huston, J. Penney, J. M. Bonner, L.-H. Tsai
Picower Institute for Learning and Memory
Department of Brain and Cognitive Sciences
Massachusetts Institute of Technology
Cambridge, MA 02139, USA
E-mail: lhtsai@mit.edu

J. L. Andresen
Department of Chemistry
Massachusetts Institute of Technology
Cambridge, MA 02139, USA

The ORCID identification number(s) for the author(s) of this article can be found under https://doi.org/10.1002/adma.202309225

DOI: 10.1002/adma.202309225

J. L. Andresen, R. Langer
Koch Institute for Integrative Cancer Research
Massachusetts Institute of Technology
Cambridge, MA 02139, USA
E-mail: rlanger@mit.edu

O. S. Fenton
UNC Eshelman School of Pharmacy
Department of Pharmacoengineering and Molecular Pharmaceutics
University of North Carolina
Chapel Hill, NC 27599, USA
E-mail: osfenton@unc.edu

R. Langer
Department of Chemical Engineering
Massachusetts Institute of Technology
Cambridge, MA 02139, USA

L.-H. Tsai
Broad Institute of MIT and Harvard
Cambridge, MA 02139, USA

PU.1 levels act as a risk factor in AD progression,[11–14] while reduced PU.1 expression is thought to be protective in humans as well as in models of AD.[11,13–17]

RNA therapeutics, including short interfering RNA (siRNA) designed to degrade mRNAs and/or impair translation to reduce target protein production, could provide a therapeutic avenue to ameliorate AD-associated transcription and translation changes in microglia. However, due to their large size and charge, nucleic acids require delivery vehicles or alternate methods of administration[18,19] to enter cells across the cellular membrane.[20] Furthermore, systemically administered drugs are often incapable of reaching the affected brain regions due to poor penetration across the blood–brain barrier (BBB). Microglia have been particularly hard to target for poorly understood reasons, which both hampers experimental studies and is an impediment to therapeutic delivery.[21,22] Four-component lipid nanoparticle (LNP) systems composed of ionizable lipid, cholesterol, phospholipid, and polyethylene glycol (PEG)-lipid conjugates have been widely implemented in COVID-19 vaccines and highlight the immense potential of RNA delivery for therapeutic purposes.[23–25] These four-component LNP systems represent the clinical gold standard of delivery vehicles for therapeutic nucleic acids. When LNPs are administered intravenously (i.v.), the corona of serum proteins which adsorb to the nanoparticle surface within the bloodstream targets them to the liver, primarily through ApoE-receptor mediated uptake.[26–28] Several nanoparticle systems and LNP modifications have been designed to improve delivery across the BBB.[29–31] Alternatively, local injections of LNPs have been shown to successfully deliver mRNA into neurons and astrocytes.[32] Recently, researchers identified cationic liposomes, lipid hybrid, and polymeric nanoparticles that can be administered locally or intranasally to transfect specific cell types such as microglia within the brain.[33–35] In addition, studies using hyaluronic acid to functionalize the LNP surface have been used to aid delivery of siRNA to glioma in mice.[36] However, clinically relevant four-component LNP systems remain underexplored for localized RNA delivery into microglia.

Here, we sought to examine the potential of LNP-facilitated delivery of RNA constructs to mitigate PU.1-mediated neuroinflammation in models of AD. We started with a small-scale screen of seven varying LNP formulations designed to optimize mRNA delivery in cell cultures of human induced pluripotent stem cell (iPSC)-derived microglia-like cells (iMGLs) and within the mouse brain after local intrathecal injection. Then, the optimal formulation was used to deliver anti-PU.1 siRNA to mouse models of systemic or AD-associated neuroinflammation. These treatments reduced neuroinflammation and further validated PU.1 as a target pathway for potential therapeutic relief in AD or other neurodegenerative and neuroinflammatory diseases.

2. Results and Discussion

2.1. Commercial Lipoplex Transfection Reagents Are Not Effective in iMGLs

We first determined if any of eight different commercially available transfection reagents could be used to efficiently deliver siRNA to human induced pluripotent stem cell (iPSC)-derived microglia-like cells (iMGLs) without causing nonspecific cytotoxicity. For an in vitro system, we chose iMGLs, which have been established as an effective model for the study of AD-associated inflammation in human microglia.[9,37–40] The identity of the iMGL cultures was validated morphologically, by immunocytochemistry with the microglia marker IBA1, and by flow cytometry with the microglial membrane protein CD11b (Figure S1a, Supporting Information). To determine cytotoxicity of the eight commercial transfection reagents, we delivered nontargeting scrambled siRNA to iMGLs and, as a control, to iPSC-derived astrocytes (iPS astrocytes, validation shown in Figure S1b, Supporting Information). Four of the eight reagents reduced iMGL viability 2 d post-treatment (Mirus 2020, $P \leq 0.0047$; Fugene6, $P = 0.0027$, DharmaFECT, $P = 0.0008$; RNAiMAX, $P = 0.0001$; **Figure 1a**), while no significant effect on viability was seen in iPS astrocytes ($P > 0.05$; Figure 1b). This confirms our qualitative observation that microglia are particularly sensitive to nonspecific toxicity from transfection reagents. We then investigated the eight commercial reagents for their ability to deliver a targeting siRNA to iMGLs, choosing an anti-PU.1 siRNA that targets the myeloid-specific *SPI1* gene encoding the PU.1 protein, and subsequently quantifying PU.1 mRNA levels in RT-qPCR experiments. All siRNA sequences were chemically modified and commercially available. Only RNAiMAX lipofectamine (RNAiMAX) significantly reduced PU.1 levels ($P = 0.0002$; Figure 1a). No effect on viability was seen in iPS astrocytes for the anti-PU.1 siRNA ($P > 0.05$; Figure 1b). Together, these findings show that none of the eight tested commercial transfection reagents are capable of efficient RNA delivery to iMGLs without causing nonspecific toxicity.

2.2. Potent MG-LNP RNA Delivery to iMGLs Can be Achieved In Vitro

Given that LNPs have shown significant therapeutic potential as a delivery vehicle in vitro and in vivo,[41,42] we next examined seven microglia LNP formulations for their ability to deliver RNA to iMGLs without causing cellular toxicity.[43] The seven LNP formulations (A to G; Figure 1c and Table S1, Supporting Information) were created by changing the structure of the ionizable lipid, the type of phospholipid, or the modified lipid-to-RNA ratios in a previously identified base formulation.[44] Recent efforts have used strategies including changing the structure of the ionizable lipid, the type of phospholipid, or alterations of the lipid:mRNA ratios to identify lead LNP for a particular route of administration.[45–47] Initial delivery experiments with the LNP used firefly *Luciferase* mRNA to allow for rapid quantitation of delivery efficacy by measuring luminescence. Dosing volume was adjusted accordingly depending on overall RNA concentration and encapsulation efficiency (EE%) of LNP to ensure equal amounts of RNA between groups. Transfection with all LNP formulations containing ionizable lipid (formulations A, B, E–G containing either cKK-E12 or 1,2-dioleoyl-3-trimethylammonium propane [DOTAP]) gave rise to luminescence in iMGL cultures 1 d after transfection (Figure 1d). We also found that incorporation of 5-methoxyuridine (5moU) modifications within the *Luciferase* mRNA transcript led to approximately threefold increase in protein expression in iMGLs 1 d after transfection with LNP formulation A ($P \leq 0.0001$), indicating reduced immunogenicity

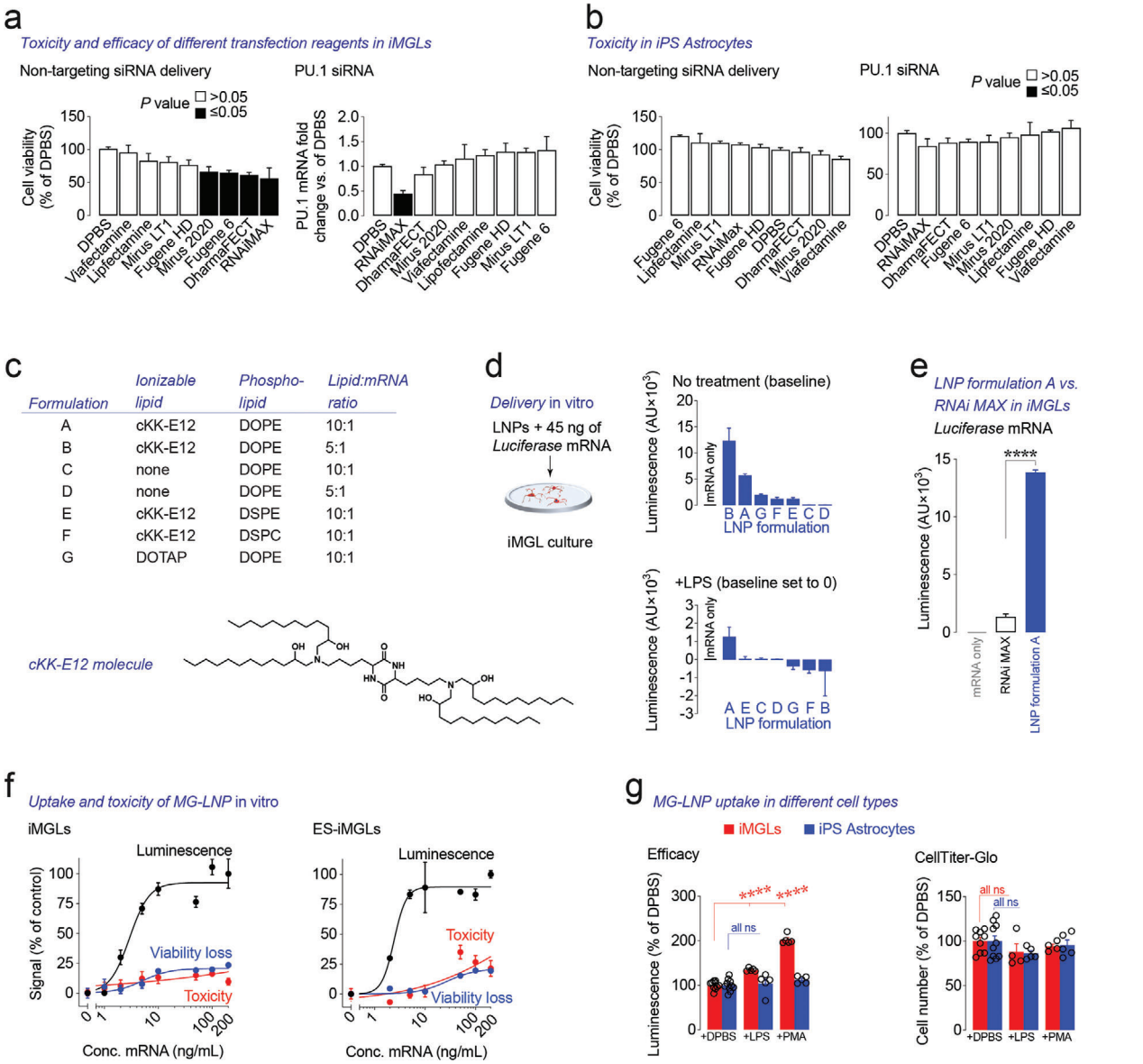

Figure 1. In vitro LNP screen to evaluate mRNA delivery in human iMGLs. Comparison of eight commercially available transfection reagents in iMGLs and iPS astrocytes for delivery efficacy and nonspecific toxicity. a) Left: nonspecific toxicity after delivery of nontargeting siRNA measured by changes in cell viability using CellTiter-Glo and right: efficacy of delivery of anti-PU.1 siRNA by measuring PU.1 mRNA levels by use of RT-qPCR 1 d after delivery. ANOVA, Dunnett's post hoc against DPBS treatment. $n \leq 4$ for all conditions. b) Same experiments as in (a) but with iPS astrocytes. ANOVA, Dunnett's post hoc against DPBS treatment. $n \leq 4$ for all conditions. c) LNP formulation variations focused on ionizable lipid and phospholipid composition, as well as lipid:mRNA ratio. Below: Structure of lead ionizable lipid, cKK-E12. d) Luminescence detected in iMGLs without (top) or with (bottom) pretreatment with 25 ng mL^{-1} LPS and incubated for 1 d with LNP encapsulating 45 ng of *Luciferase* mRNA. e) *Luciferase* mRNA delivery efficiency of LNP relative to RNAiMAX in iMGLs. Student's unpaired, two-sided *t*-test, ****$P \leq 0.0001$. $n \geq 3$ for all conditions. f) Dose–response titration from 1 to 200 ng mL^{-1} *Luciferase* mRNA encapsulated by MG-LNP, evaluating luminescence, viability loss, and toxicity in iMGLs (left) and ES iMGLs (right) derived microglia, curves were fitted using Hill's equation. g) Comparison of percent luminescence of DPBS-treated cells (left, using BrightGlo in order to determine expression levels of Luciferase) and cell number (right, using CellTiter-Glo in order to determine cell viability) upon LNP delivery in iMGLs (red) and iPS astrocytes (blue) after a 2-d pretreatment with the pro-inflammatory molecules LPS or PMA. Student's unpaired, two-sided *t*-test, ****$P \leq 0.0001$. $n \geq 3$ for all conditions.

of the modified RNA (Figure S1c, Supporting Information).[48,49] The use of modified mRNA was also found to have no impact on cell viability compared to unmodified mRNA while increasing protein expression. All subsequent experiments with *Luciferase* mRNA had the 5moU modification.

Since delivery of genetic material into inflammatory microglia is of particular interest for the treatment of AD,[7] we also determined the efficiency of LNP-mediated *Luciferase* mRNA delivery to iMGLs pretreated with the pro-inflammatory molecule lipopolysaccharide (LPS) for 2 d to induce inflammation.

Pre-treatment with LPS did not affect viability for any of the formulations (Figure S1e,f, Supporting Information, cells cultured in the presence of 1×10^{-6} M Actinomycin D for 24 h were used as positive control for cell death, see "dead" column). LNP formulation A (named MG-LNP) demonstrated a significantly higher delivery efficiency in LPS-treated iMGLs, with ≈24% more luminescence than formulation A without LPS, $P = 0.044$ (Figure 1d and Figure S1g, Supporting Information), while the other LNP formulations exhibited similar or even reduced delivery efficiencies in LPS-treated versus control iMGLs (Figure 1d and Figure S1g, Supporting Information). A notable example is formulation B, which showed higher delivery efficacy than MG-LNP, but a reduction after LPS treatment, making it less suitable for targeting inflammatory microglia. MG-LNP also showed increased delivery efficiency in iMGLs pre-treated with a second pro-inflammatory molecule, phorbol myristate acetate (PMA ≈ 35%, $P = 0.006$; Figure S1g, Supporting Information).

MG-LNP not only showed the most promising RNA delivery efficiency in both untreated and pro-inflammatory iMGLs among the tested LNP formulations, but also tenfold higher delivery efficiency than RNAiMAX in untreated iMGLs (Figure 1e). Therefore, we focused additional characterization experiments on this formulation. MG-LNP generated luminescence signal in iMGLs within only 2–3 h after delivery (Figure S1d, Supporting Information, left). The luminescence signal peaked at 24 h postdelivery and remained steady for 4 d (Figure S1d, Supporting Information, right). We then titrated MG-LNP in iMGLs and a second line of embryonic stem cell (ES)-derived MGLs from 1 to 200 ng of encapsulated *Luciferase* mRNA (equivalent to concentrations of $0.02–4 \times 10^{-9}$ M). We observed that delivery efficiency (as measured by luminescence) plateaued at ≈10 ng mL^{-1}, with negligible cell toxicity and/or loss of viability observed at doses up to 50 ng (as measured by MultiTox assay; Figure 1f). We also evaluated the MG-LNP in iPS astrocytes treated with the pro-inflammatory molecules LPS or PMA. In contrast to iMGLs, iPS astrocytes did not show a detectable change in the overall level of luminescence after MG-LNP-mediated mRNA transfection ($P > 0.05$; Figure 1g). These results indicate that MG-LNP robustly delivers mRNA to microglia and other brain cell types, such as astrocytes. In addition, the increased luminescence signal in LPS pretreated iMGLs but not in LPS pretreated iPS astrocytes, suggests our MG-LNP offers a degree of increased transfection efficacy in microglia during inflammation.

2.3. Localized Delivery of LNP Formulation A In Vivo Efficiently Transfects Cells of the Brain

Although MG-LNP emerged as the most promising transfection reagent for iMGL cultures, in vitro transfection results are not always predictive of in vivo performance, often necessitating more costly in vivo screening experiments.[50,51] We evaluated the delivery efficacy in vivo for all seven LNP formulations. Previous reports on i.v. administration of MG-LNP demonstrated predominant expression of the transfected RNA (>90%) within the liver and with little penetration across the BBB.[28,52] We therefore injected LNPs intracisternally (i.c.st.) in order to bypass the BBB and deliver RNA directly into the cerebrospinal fluid through the foramen magnum of the mouse.[32,35,53–55] C57BL/6J mice were injected either intraperitoneally (i.p.), as a control, or i.c.st. with 0.5 and 0.07 mg kg^{-1}, respectively, with LNP-encapsulated *Luciferase* mRNA (**Figure 2a,b**), where the smaller dose used for i.c.st. injection was due to volume limitations of the cerebrospinal fluid compartment. One day after injection, liver and brain were dissected, homogenized, and analyzed for luminescence. We observed no obvious side effects of the LNP treatment in the mice. Following i.p. injection, several LNP formulations achieved robust luminescence in the liver. MG-LNP also showed luminescence signal in brain tissue indicating that MG-LNP was able to cross the BBB to some extent. However, luminescence signal detected in the brain from treatment with MG-LNP was nearly an order of magnitude less than in the liver. Administration of MG-LNP by i.c.st. led to a twofold greater luminescence within the brain compared to i.p. administration; 1.4 ± 0.6 versus i.p.: 0.67 ± 1.2 luminescence units (Figure 2a,b, see "Whole brain" for MG-LNP). Comparable signal was detected for several other LNP formulations (Figure 2a,b). Strikingly, all LNP formulations outperformed the commercially available reagent Invivofectamine, designed for delivery of genetic material into mice, regardless of injection route and target organ.

We then ranked the overall delivery efficacy for the different LNP formulations both in vitro in iMGLs and in vivo in brain and liver after averaging i.c.st and i.p. injection (Figure 2c). Remarkably, we observed a strong correlation between in vitro and in vivo ranks, suggesting that our in vitro results were predictive of in vivo results, in particular for MG-LNP, which stood out as the highest performing formulation for both measures. Future work will be necessary to further validate whether the observed in vitro and in vivo correlation remains predictive for other LNP systems. Given the favorable performance of MG-LNP, we compared its i.p. and i.c.st. delivery efficacy of *Luciferase* mRNA in various organs (Figure 2e). We found that i.p. injection targeted peripheral organs preferentially while i.c.st. preferentially targeted the brain. We then dissected various brain regions in order examine the distribution across the brain (Figure 2f). After i.c.st injection with MG-LNP, luminescence was detected throughout the brain, with the strongest signal observed closest to the injection site in the brainstem. I.p. injection consistently yielded lower luminescence values in the brain compared to i.c.st., with the strongest signal detected in the cortex. These results indicated that an i.c.st. route of delivery will preferentially target brains regions over peripheral organs.

2.4. MG-LNP Acts as a Potent Delivery Vehicle for Anti-PU.1 siRNA In Vitro

We next used our MG-LNP to deliver anti-PU.1 siRNA instead of *Luciferase* mRNA to iMGLs (Table S1, Supporting Information). MG-LNP delivery of anti-PU.1 siRNA achieved a concentration-dependent reduction in PU.1 mRNA levels, with doses of 200 ng mL^{-1} generating a 42 ± 25% decrease as quantified by RTqPCR (**Figure 3a**, left panel). In addition to being involved in pro-inflammatory signaling, the PU.1 gene is necessary for the survival of immune cells such as microglia[10] and knockdown of PU.1 leads to the death of microglia in vitro over time (Figure 3a, right panel). By comparison, transfection with RNAiMAX required a fivefold higher dose (1000 ng mL^{-1}) to achieve similar

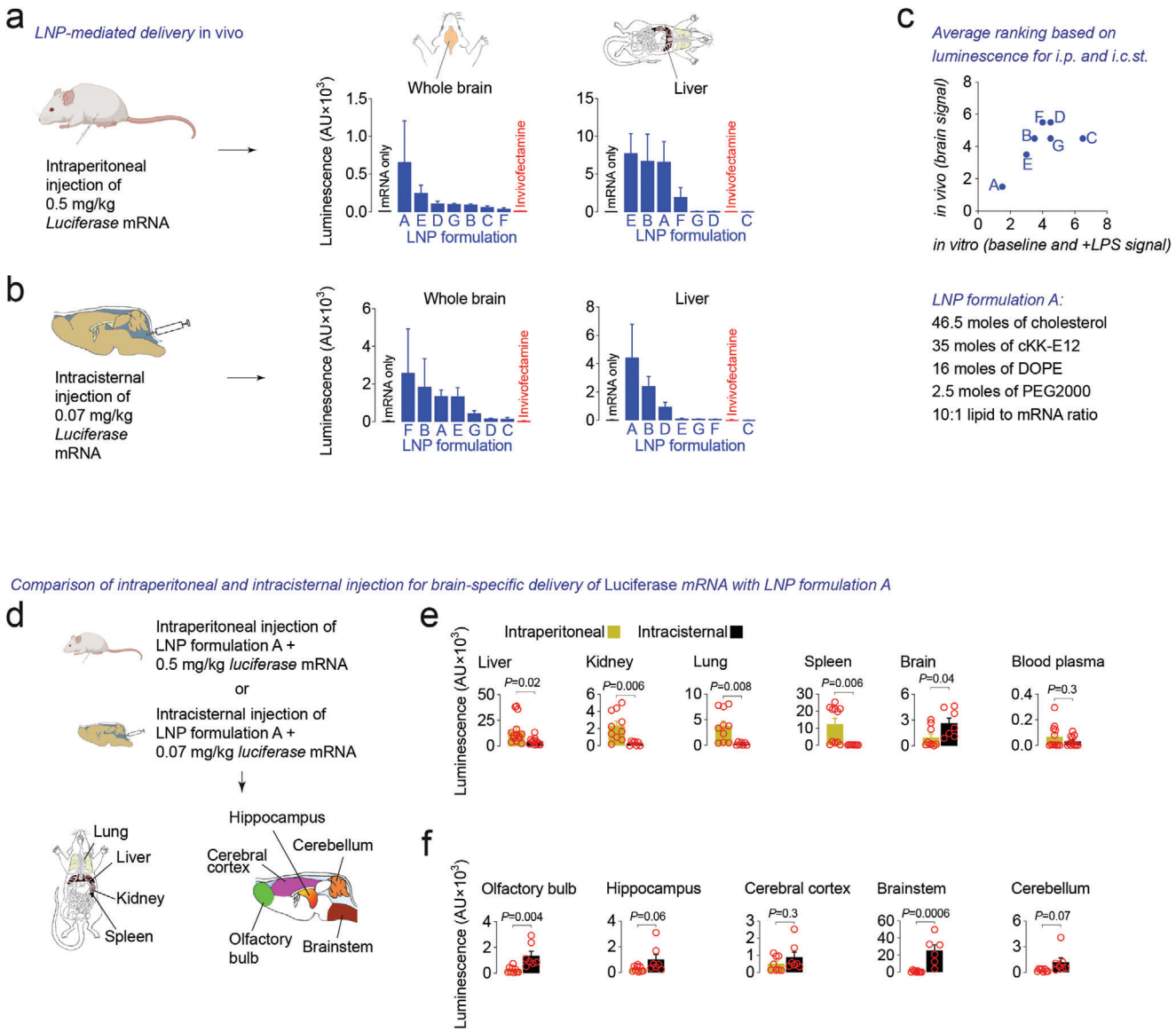

Figure 2. Delivery of mRNA via local or systemic mRNA-LNP injection. Schematic demonstrating a) intraperitoneal (i.p.) administration or b) intracisternal (i.c.st) administration of delivery vectors containing *Luciferase* mRNA. One day after injection, luminescence in resected and homogenized whole brain or liver samples was measured. The commercially available in vivo transfection reagent Invivofectamine was included as a reference. c) Composite ranking of the various LNP formulations A–G across in vitro and in vivo delivery performance in Figure 1d and Figure 2a,b. The *y*-axis shows average ranking for i.p. and i.c.st. injection with regard to mouse brain luminescence signal for each formulation. The *x*-axis shows average luminescence signal in iMGLs, ranked as an average of the baseline condition and with LPS added. d) Luminescence signal in internal organs and regions of the brain after i.p. (yellow bars) or i.c.st. (black bars) delivery of *Luciferase* mRNA-LNP into wildtype, C57BL/6J mice 1 d after delivery. Organs were resected and homogenized prior to luminescence measurements. Student's unpaired, two-sided *t*-test. $n \geq 6$ for all conditions.

effects (52 ± 50%). MG-LNP delivery of anti-PU.1 siRNA at 500 ng mL^{-1} achieved PU.1 transcriptional silencing up to 92 ± 2% within 12 h without concurrent increase in cell death (Figure 3a, middle and right panel), which only became evident after 2 d of PU.1 silencing (Figure 3a, right panel). In addition, we explored a number of known PU.1 target genes[13] and observed a strong reduction of transcript levels of inflammatory microglial markers, including *TREM2, TNFA*, and *IL1B*, within 2 d of MG-LNP delivery of anti-PU.1 siRNA (Figure 3a,b).[13] We also confirmed our findings in iMGLs derived from embryonic stem cells (see ES-iMGLs, Figure 3b). In accordance with findings in mouse microglia, we observed significantly increased levels of *APOE* transcription upon PU.1 silencing in iMGLs (Figure 3b).[13] Immunocytochemistry staining of iMGLs with a PU.1 antibody confirmed the successful knockdown with anti-PU.1 siRNA as compared to a scrambled nontargeting siRNA control (Figure 3c). We further validated the superior delivery efficacy and lack of cytotoxicity of MG-LNPs compared to RNAiMAX through flow cytometry. We observed no significant drop in PU.1 expression (91 ± 14% of DPBS-treated iMGLs) upon LNP delivery of

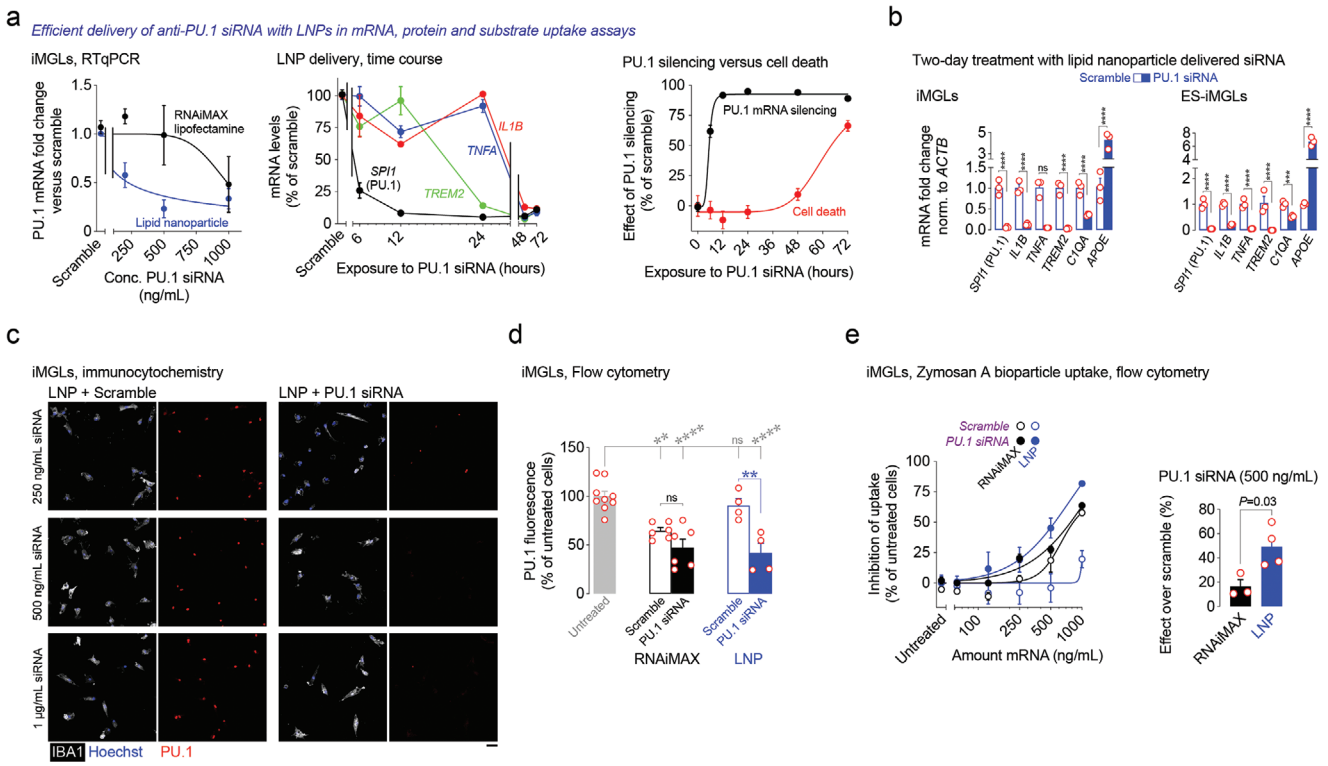

Figure 3. MG-LNP knockdown of PU.1 alters target gene expression and function in human iMGLs. a) Left: Concentration-response curve in RTqPCR experiments—showing SPI1 levels (the gene for PU.1) normalized to ACTB—comparing delivery of siRNA with RNAiMAX (black circles) and MG-LNP (blue symbols). Curves were fitted using Hill's equation. Middle: RTqPCR experiments on various genes, normalized to ACTB, over time after delivery of anti-PU.1 siRNA using LNPs. Right: Time course of cell death (red circles) after PU.1 silencing (black circles). Cell death was measured with CellTiterGlo. b) RTqPCR after delivery of anti-PU.1 siRNA (PU.1 siRNA) versus nontargeting siRNA (Scrambled), side-by-side in iMGLs (left) and ES iMGLs (right), normalized to ACTB. Student's unpaired, two-sided *t*-test performed on cycle numbers, $^{****}P \leq 0.0001$, $^{***}P \leq 0.001$, $n \geq 3$ for all data points. Bars are mean ± SEM, each data point represents one well. c) Immunocytochemistry of iMGLs treated with LNPs carrying either scrambled siRNA (left) or anti-PU.1 siRNA (right), staining for cytoplasmic IBA1 and nuclear PU.1, counterstained with Hoechst. d) Flow cytometry using a PU.1 antibody, comparing RNAiMAX and LNPs containing either scramble or anti-PU.1 siRNA. Student's unpaired, two-sided *t*-test performed on cycle numbers, $^{****}P \leq 0.0001$, $^{**}P \leq 0.01$. Bars are mean ± SEM, each data point represents a well. e) Left: concentration response curve, comparing delivery with RNAiMAX Lipofectamine and LNPs, right: quantification at 500 ng mL^{-1}. Student's unpaired, two-sided *t*-test.

scramble siRNA while we saw a robust reduction of 42 ± 20% after anti-PU.1 siRNA delivery (Figure 3d). In contrast, RNAiMAX-mediated delivery of scrambled siRNA already reduced fluorescence by 35 ± 8%, compared to 53 ± 21% after anti-PU.1 siRNA delivery, again indicating nonspecific cellular toxicity from the transfection reagent. Given that increased PU.1 activity correlates with microglial engulfment activity,[57] we then used microglial uptake of fluorescently labeled Zymosan A-coated bioparticles as a functional measure of PU.1 inhibition in flow cytometry experiments. RNAiMAX-mediated delivery of scrambled siRNA complexes again caused a nonspecific reduction in uptake starting at 250 ng mL^{-1}, while MG-LNP-mediated delivery only affected uptake at concentrations ≥1000 ng mL^{-1} (see open black vs blue circles, Figure 3e). Simultaneously, MG-LNP-mediated delivery of anti-PU.1 siRNA consistently resulted in a greater reduction in uptake than RNAiMAX-mediated delivery of anti-PU.1 siRNA at equivalent doses. Together, these results show that LNPs are more efficient at delivering siRNA and better tolerated in iMGLs than commercially available reagents (Figure 3e). These findings support the potential use of MG-LNP-mediated anti-PU.1 siRNA delivery as a potential therapy for neuroinflammatory diseases.

2.5. MG-LNP Delivery of Anti-PU.1 siRNA by Localized Injection Reduces Neuroinflammation in Mice

We used two different mouse models of neuroinflammation to test the effect of localized MG-LNP-delivery of anti-PU.1 siRNA: 1) an LPS-induced model of systemic inflammation, and 2) the inducible CK-p25 model of neurodegeneration and neuroinflammation.[13] Although PU.1 is encoded by *Spi1* in humans, the homologous gene in mice is *Sfpi1*, requiring a change in sequence in the anti-PU.1 siRNA selected for in vivo experiments. We first validated efficiency and tolerability of MG-LNP-encapsulated anti-PU.1 siRNA targeted against the mouse *Sfpi1* gene by transfecting a BV2 mouse microglia cell line (BV2-PU.1-Luciferase cells) which expresses a PU.1-activity dependent *Luciferase* reporter construct.[17] With these cells, LNPs containing scrambled siRNA control caused no change in luminescence (Figure S2, Supporting Information), whereas MG-LNPs delivering anti-PU.1 siRNA reduced luminescence in a concentration dependent manner from ≥10 ng mL^{-1} on.

To establish a mouse model of systemic inflammation, we injected six-week-old male C57BL/6J wildtype mice i.p. with LPS

at 10 mg kg^{-1} (Figure S3a, Supporting Information). After 1 d, LPS-treated mice showed a profound reduction in locomotion in an Open Field arena, from 34 ± 9 to 1.4 ± 0.9 m ($P \leq 0.0001$) traveled in 10 min (Figure S3b, Supporting Information). LPS treatment also increased immune cell infiltration of hepatic vessels in hematoxylin and eosin-stained liver sections, seen as the presence of red-stained immune cells at the circumference of the vessel wall 1 d after injection. LPS-injected mice exhibited 28 ± 18% infiltrated vessels per liver section versus 5 ± 6% in saline injected mice ($P \leq 0.002$, Figure S3c, Supporting Information). LPS injection also increased neuroinflammatory markers in the hippocampus of mice one day later (Figure S3d, Supporting Information). The number of PU.1-positive nuclei per field of view was increased 2.5-fold in the dentate gyrus in LPS-injected mice ($P \leq 0.0001$), indicating microglial proliferation. Microglial surface area immunoreactivity of IBA1 was increased by 3.5-fold ($P \leq 0.0001$) as well, indicating microglial activation. In addition, C1Q-positive area rose 2.3-fold ($P = 0.01$), and astrogliosis, as measured by GFAP immunoreactive surface area, was up 1.7-fold ($P = 0.02$).

We evaluated the effect of PU.1 knockdown in this model of systemic inflammation by pairing the LPS injection with either i.p. or i.c.st. injection of MG-LNP with anti-PU.1 siRNA. In both treatment groups, reduced mouse locomotor activity during the 10-min test period was partially alleviated, with the strongest effect seen after i.p. administration (i.p.: 4m ± 1m, $P \leq 0.005$ vs i.c.st.: 3m ± 0.8m, $P \leq 0.05$; **Figure** 4a), indicating that ongoing inflammation in the periphery can contribute to reduced locomotor activity in mice. In order to assess the degree of inflammation in the periphery, we investigated the liver of the mice injected with LPS and the MG-LNPs. Inflammation of the liver is associated with the presence of infiltrating monocytes that stain blood vessels red after immersion in hematoxylin & eosin reagent.[56] Both i.p. and i.c.st. injection of LNPs with anti-PU.1 siRNA reduced the percentage of red-stained vessels per field of view (black arrows) as compared to injection of MG-LNP with scrambled siRNA (yellow arrows). As expected, the i.p. injection of MG-LNPs with anti-PU.1 siRNA conferred a stronger anti-inflammatory effect in the periphery than i.c.st. injection, leading to a 66 ± 11% decrease ($P = 0.01$) in red-stained vessels compared to only a 15 ± 16% decrease for i.c.st. ($P = 0.05$) relative to mice treated with LPS and nontargeting siRNA (Figure 4b,c).

We subsequently performed RTqPCR on resected whole brain, liver, and spleen in order to examine the transcriptional changes induced by LPS injection. We found that *Sfpi1* and the downstream inflammatory genes *Il1b* and *Ccl2* were strongly upregulated in all three tissues 1 d after LPS treatment (max values normalized to two for display purposes; Figure 4d, for raw data see Figure S4a,b, Supporting Information). In brain tissue, both i.c.st. and i.p. injection of anti-PU.1 siRNA MG-LNP achieved significant knockdown of *Sfpi1* (5.7- and 1.2-fold decrease, respectively), *Il1b* (4.2- and 1.9-fold decrease, respectively) and a reduction in *Ccl2* (2.4- and 4.9-fold decrease, respectively) mRNA transcripts. Notably, i.c.st. injections did not result in a significant knockdown in the peripheral organs, while i.p. injections did. In the liver, i.c.st and i.p. injections resulted in 1.2- and 4.3-fold decreases in *Sfpi1* RNA, respectively; 0.8- and 4.2-fold decreases in *Il1b* RNA, respectively; and 1.0- and 2.9-fold decreases in *Ccl2* RNA, respectively. Similar effects were seen in homogenized spleen tissue, where i.c.st and i.p. administration led to a 1.4- and 4.2-fold decreases in *Sfpi1* RNA, respectively; 0.9- and 8.1-fold decreases in *Il1b* RNA, respectively, and *a* 1.0- and 4.5-fold decreases in *Ccl2* RNA, respectively.

Confocal microscopy of hippocampal brain slices of mice injected with LPS that were stained with a PU.1 antibody indicated a comparable reduction in the number of PU.1-positive nuclei per field of view after anti-PU.1 siRNA delivery by i.p. (from 49 ± 12 to 32 ± 12, $P = 0.02$) or i.c.st. (from 38 ± 7 to 30 ± 7, $P = 0.02$) (Figure 4e). Similarly, quantification of the microglial markers IBA1, C1Q, and astrocytic GFAP by immunohistology showed a reduction by 42% for IBA1 ($P = 0.02$), 84% for C1Q ($P = 0.0008$) and 44% for GFAP ($P = 0.03$) after i.p. injection with anti-PU.1 siRNA. Furthermore, i.c.st. injection reduced the immunoreactivity of these markers, although to a lesser degree, with statistical significance only reached for C1Q (69% reduction, $P = 0.03$) and GFAP (27% reduction, $P = 0.03$; Figure 4f). I.p. injection of anti-PU.1 siRNA results in a broad reduction in PU.1 expression and downstream markers across all organs measured, including the liver and spleen. In contrast, the significant reduction in PU.1 expression as measured by RTqPCR upon i.c.st. injection is localized solely within the brain. The increased efficacy of i.p. delivered MG-LNPs could be due to the fact that LPS was injected systemically and involves the peripheral immune system, combined with the fact i.p. injection allows for larger injection volumes.

Finally, we evaluated the anti-inflammatory potential of MG-LNP-mediated PU.1 knockdown in a transgenic CK-p25 mouse model of chronic neuroinflammation, which mimics the neuroinflammatory aspects of AD.[12,57] Rather than through induction of systemic inflammation by LPS injection, these mice express the neurotoxic CDK5 activator p25 under the control of a tamoxifen-inducible promoter specific to excitatory neurons.[13] After induction, CK-p25 mice progressively develop neurodegenerative phenotypes including a profound neuroinflammatory response by two weeks.[58] In order to determine an appropriate dosing regimen for prolonged MG-LNP-mediated PU.1 knockdown, we first used *Luciferase* mRNA to establish the time-course of protein expression after i.c.st. MG-LNP delivery. Luminescence in the liver faded completely by day 4 after i.c.st. injection (90 ± 2% reduction) while still remaining detectable in hippocampus (41 ± 12% reduction) and cortex (58 ± 9.7% reduction) tissue (Figure S4c, Supporting Information). By day 7, luminescence in hippocampus and cortex had fallen to below 10%. Based on these results, we treated CK-p25 mice every third day during the two-week induction period (on days 0, 3, 6, 9, 12) with i.c.st. MG-LNPs encapsulating either scrambled or anti-PU.1 siRNA (Figure S4d, Supporting Information). After 14 d, animals were sacrificed and hippocampal tissue was assessed for neuroinflammatory markers. In CK-p25 mice injected with anti-PU.1 siRNA, the presence of PU.1-positive cells was nearly reduced to baseline control levels (from 66 ± 10 to 32 ± 17 nuclei, $P = 0.001$; Figure 4g, with quantification in Figure 4h). Additional anti-inflammatory effects manifested as reduction in hippocampal immunoreactivity of the microglial markers IBA1 by 61% ($P = 0.01$), C1Q by 62% ($P = 0.02$), and astrocytic GFAP by 39% ($P = 0.03$). We imaged the hippocampus after the two-week p25-induction course in control mice or

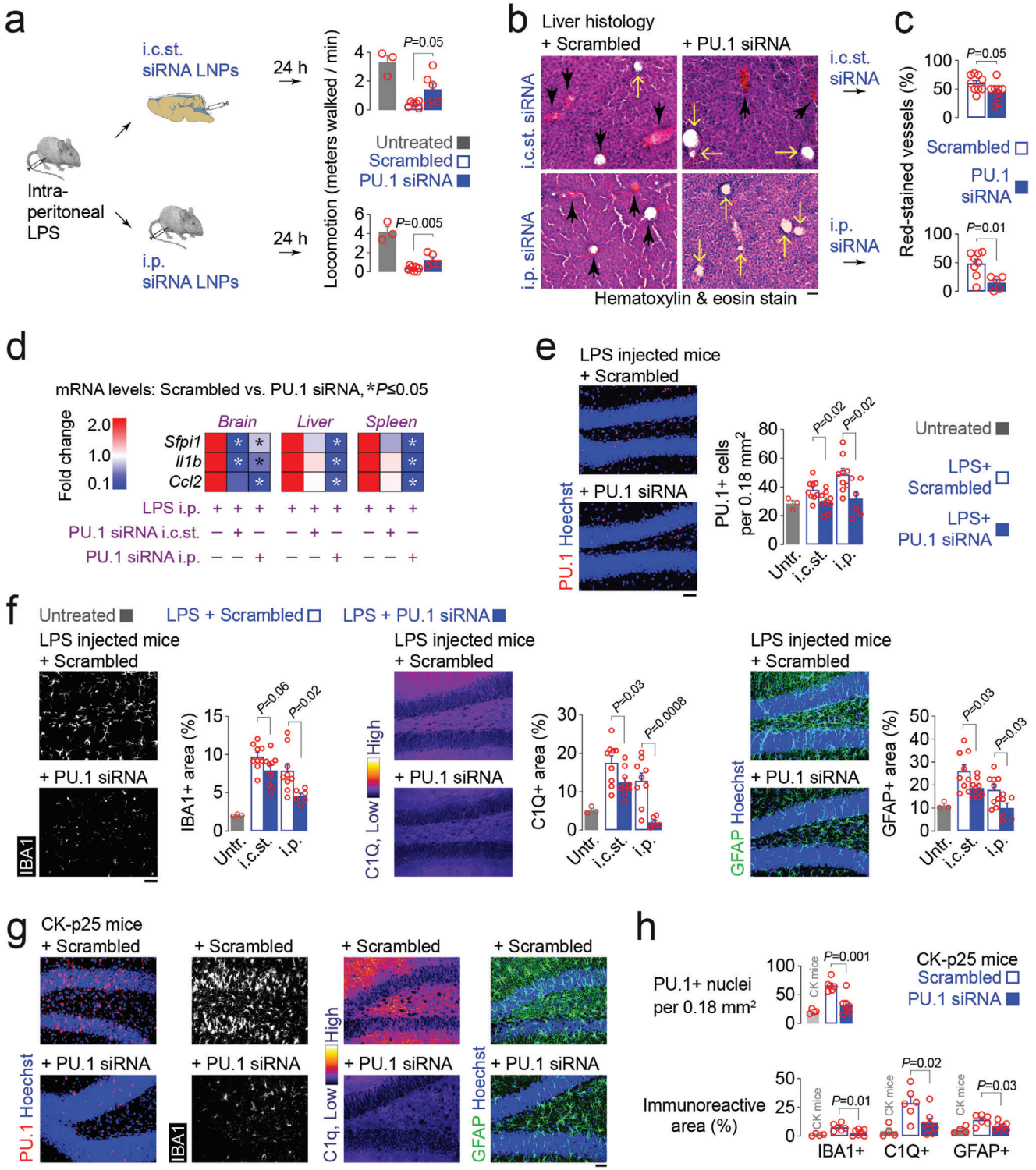

Figure 4. Silencing PU.1 with MG-LNP is anti-inflammatory during acute systemic inflammation and neurodegeneration. a) Left: schematic of in vivo mouse experiments. LPS was injected at 10 mg kg^{-1} i.p., immediately followed by i.c.st. (top) or i.p. (bottom) injection of MG-LNP containing either nontargeting siRNA (Scrambled, open blue bars) or anti-PU.1 siRNA (PU.1 siRNA, filled blue bars). One day later, mice were placed in the Open Field arena and had their general locomotor activity measured over 10 min. Student's unpaired, two-sided *t*-test. b) Liver sections stained with hematoxylin and eosin after i.c.st. (top) or i.p. injection (bottom) of LNPs encapsulating nontargeting or anti-PU.1 siRNA. Black arrows indicate vessels (defined as intact, circular, and empty structures of ≈40 µm size) with accumulation of immune cells (red stain). Yellow arrows indicate vessels not containing accumulated immune cells. Scale bare is 40 µm. c) Quantification. Student's unpaired, two-sided *t*-test. d) Comparison levels of *Sfpi1*, *Il1b*, and *Ccl2* mRNA transcripts as determined by RTqPCR, normalized to *actb*, in whole brain, liver, and spleen tissue after i.p. LPS administration and i.p. and i.c.st. LNP injection. Student's unpaired, two-sided *t*-test performed on cycle numbers. e) Confocal micrographs of hippocampal tissue stained for PU.1-

mice concomitantly injection course of LNP vehicle containing scrambled siRNA. When compared to control saline injections, there was no change in expression in these inflammatory microglial markers, indicating the LNP delivery vehicle was well-tolerated and did not induce any obvious inflammation (Figure S5, Supporting Information). Taken together, these results indicate that MG-LNP delivery of anti-PU.1 siRNA can potentially be used as an anti-inflammatory therapeutic in mice with systemic inflammation and in the CK-p25 mouse model of AD-associated neuroinflammation.

3. Conclusions

In this article, we highlight the need for novel reagents to facilitate delivery of nucleic acids, including mRNA and siRNA, for basic research as well as for investigating potential therapeutics in microglia. Microglia, the main immune cells of the brain, represent an attractive target for neurodegenerative disorders. They express a majority of the AD risk genes identified in genome wide association studies for AD[9] and are critical mediators of neuroinflammation, a pervasive hallmark of all neurodegenerative diseases.[1] However, immune cells are notoriously challenging to transfect in vitro and in vivo. Through a small-scale screening of LNP formulations, we identified an LNP formulation, labeled MG-LNP, that delivered mRNA or siRNA cargo more effectively and with less cytotoxicity than commercial reagents to iMGLs in vitro and to microglia of the mouse brain in vivo. Upon localized i.c.st. injection in mice, MG-LNP yielded detectable luminescence in all regions of the brain with less exposure in peripheral organs as compared to an i.p. injection. Furthermore, this formulation exhibited enhanced delivery to iMGLs following treatment with pro-inflammatory molecules.

We further examined the role of the AD-risk locus and master regulator of inflammation, PU.1, in LPS-treated and CK-p25 mice. Our findings demonstrate that PU.1 is a promising target for anti-inflammatory siRNA therapeutics. Delivering anti-PU.1 siRNA with our MG-LNP to LPS-injected mice resulted in reduced systemic inflammation in LPS-injected mice, as measured by reduced immune cell infiltration of the liver, lowered expression levels of PU.1 in brain, spleen and liver, and dampened markers of downstream microglial activation in the brain. In the CK-p25 mouse models of neuroinflammation, repeated LNP-mediated i.c.st. delivery of anti-PU.1 siRNA also reduced neuroinflammatory hallmarks close to levels seen in control mice. We demonstrate proof-of-principle that MG-LNP mediated delivery of siRNA can ameliorate the neuroinflammatory hallmarks that are often observed in neurodegenerative diseases with associated microglial hyperactivation.

More broadly, delivery of RNA by MG-LNP can be used to examine the effects of genetic perturbations in microglia cultures and to identify novel therapeutic gene targets in other cell types. Additional formulation optimization may reveal LNP candidates which significantly improve delivery efficacy even after systemic injection by facilitating crossing of the BBB or by extending longevity of knockdown effect, ultimately obviating the need for repeated dosing. Finally, MG-LNP delivery of silencing RNA into microglia represents a novel class of therapeutics for diseases characterized by neuroinflammation, including AD and other neurodegenerative diseases.

4. Experimental Section

Human iPS and ES Microglia Experiments: Unedited human iPS (Coriell, AG09173) and ES (WiCell, WA09) cells were cultured on plates (VWR, 62406-161) coated with Matrigel (VWR, BD354277) in mTeSR1 media (STEMCELL, 85850), and lifted with ReLeSR (STEMCELL, 05872). G-band karyotyping was performed by Cell Line Genetics. iPS and ES cells were differentiated into microglia using an optimized version of a published protocol,[39] starting with the STEMdiff Hematopoietic Kit (STEMCELL, 05310) reagents for 12 d, followed by maintenance in DMEM/F12, HEPES, 2% ITS-G (ThermoFisher, 41400045), 2% B27 (ThermoFisher, 17504044), 0.5% N2, 1% Glutamax (ThermoFisher, 17502048), 1% NEAA, 1% PenStrep, 100×10^{-6} M β-mercaptoethanol (Millipore, M6250), 25 ng mL^{-1} MCSF (PeproTech, 200-35), and 100 ng mL^{-1} IL34 (PeproTech, 200-34). The cells were used between days 45 and 200 in culture. Purity of microglia cultures was assessed via flow cytometry (BD, FACSaria IIu) after washes in DPBS, blocking in FcR blocking reagent (Miltenyi, 130-059-901), and labeling with CD11b-APC (Miltenyi, 130-113-794), NeuN-488 (Millipore, MAB377X) or GLAST-PE (Miltenyi, 130-095-822). Before flow cytometry, the cells were lifted using cell scrapers (Corning, 353085) and passed through a 35 µm filter cap tube (ThermoFisher, 08-771-23). Immunocytochemistry was performed on cells plated directly on untreated glass slides (Millipore, PEZGS0816) followed by 4% paraformaldehyde fixation and a 1-h incubation in blocking solution, consisting of 5% Normal Donkey Serum (Millipore, S30-M) and 0.3% Triton-X (Millipore, T8787) in DPBS. Cells were incubated with primary antibody overnight in blocking solution, followed by three 10-min DPBS washes before exposure to a secondary antibody for 30 min at room temperature, and then three 10-min DPBS washes with 1 µg mL^{-1} Hoechst (ThermoFisher, H3570) added to the last wash. Finally, the glass coverslip was mounted using Fluoromount-G (VWR, 100502-406) and left to solidify overnight at room temperature. Confocal microscopy (Zeiss, LSM 880) was performed using a 20× Plan-Apochromat objective (Zeiss, 421452-9880-000). Luminescence was triggered with Bright-Glo reagents (Promega, E2650) and immediately measured using an EnVision Multilabel Plate Reader (PerkinElmer, 2105-0010). Toxicity and loss of viability was measured with MultiTox-Fluor Multiplex Cytotoxicity Assay (Promega, G9200), and read on the EnVision Multilabel Plate Reader, after 30 min incubation at RT. Uptake assays were

positive nuclei and all nuclei with Hoechst in LPS injected mice, co-injected i.p. with either nontargeting siRNA (top) or anti-PU.1 siRNA (bottom). Right: Quantification of PU.1-positive cells for untreated (no LPS or LNP injection) mice in gray bars ($n = 3$), LPS-injected mice co-injected with LNPs containing scrambled (empty blue bars, $n = 6$ for i.p. and 9 for i.c.st.) or anti-PU.1 siRNA (filled blue bars, $n = 6$ for i.p. and 6 for i.c.st). Student's unpaired, two-sided t-test. Scale bar is 50 µm. f) Confocal micrographs of hippocampal tissue stained for IBA1, C1Q, and GFAP and quantification of immunoreactive area for untreated ($n = 3$), treated with LPS alone ($n = 3$), and treated with LPS and scrambled or anti-PU.1 siRNA by i.p. ($n = 6$) or i.c.st. ($n = 9$) injection. g) Confocal micrographs of hippocampal dentate gyrus staining of CK-p25 mice treated with LNPs containing scrambled nontargeting siRNA (top) or anti-PU.1 siRNA (bottom). h) Quantification of mice from (f), $n = 4$, 6, and 7 for CK-p25 mice, CK-p25 mice treated with scrambled siRNA, and CK-p25 mice treated with anti-PU.1 siRNA, respectively. Student's unpaired, two-sided t-test performed between CK-p25 mice. Bars are mean ± SEM, each data point represents a well.

performed by overnight incubation of stem cell-derived microglia in clear-bottom 96-well plates (VWR, 3603) with 30 µg mL^{-1} pHrodo-labelled zymosan A bioparticles (ThermoFisher, P35365), analyzed with flow cytometry (BD, FACS Celesta HTS-1). Microglial activation was achieved by a 2-d incubation with 25 ng mL^{-1} of either IFNγ (R&D Systems, 285-IF-100), LPS (Millipore, L-2654), or PMA (Millipore, P1585-25MG). Commercially used transfection reagents were added exactly according to the instructions of the manufacturer (Lipofectamine: ThermoFisher, 18324012; Lipofectamine RNAiMAX: ThermoFisher, 13778075; Invivofectamine, ThermoFisher, IVF3001). Astrocytes were derived from human iPS (Coriell, AG09173) cells as previously described.[58]

BV2 PU.1 Reporter Cell Line: The BV2 PU.1-Luciferase reporter cell line was made by inserting five tandem copies of the λB motif,[59] followed by a minimal promoter and the luciferase coding sequence from the pGL4.23 luciferase plasmid (Promega, E8411), into the pROSA26-1 plasmid (Addgene, 21714). Then, the reporter construct was transfected into BV2 cells with lipofectamine (ThermoFisher, 18324012). BV2 cells were cultured in RPMI media (Millipore, R7388-500ML), 1% PenStrep (Wisent, 450-201-EL), 10% FBS (Gemini, 100-106) and were under constant selection with 1% G418 (ThermoFisher, 10131027), grown in CELLSTAR flasks (VWR, 82050-872), and passaged with TrypLE (ThermoFisher, 12605028).

Lipid Nanoparticle Preparation: LNP were formulated through a microfluidic mixing process as previously described.[43,60] Ionizable lipid cKK-E12 was synthesized according to previously published protocols.[28] Cholesterol, phospholipids, and PEG-lipid were purchased from Avanti Polar Lipids and stored at −20 °C prior to use. Briefly, all lipids were dissolved as stock solutions in 100% ethanol at a concentration of 10–20 mg mL^{-1}. RNA was dissolved in 10 × 10^{-3} M citrate buffer pH 3.0 at a concentration of 133 µg mL^{-1}. Lipid solutions were mixed with a 35:46.5:16:2.5 mol% ratio of ionizable lipid:cholesterol:phospholipid:PEG-lipid unless otherwise specified. The final lipid solution was calculated such that the final ratio of ionizable lipid:RNA was 10:1 unless otherwise indicated. These solutions were mixed through dual-syringe pumps at a volume ratio of 3:1 aqueous:ethanol within a microfluidic channel in a PDMS mold, resulting in LNP with a final RNA concentration of 100 µg mL^{-1}. LNP solutions were then dialyzed against 1× PBS using 20K MWCO (for mRNA) or 3.5K MWCO (siRNA) Slide-a-lyzer cassettes (ThermoFisher, 66005) at 4 °C for at least 2 h. After dialysis, LNP aliquots were removed for characterization, and the remaining solution was stored at 4 °C until dosing experiments were performed in vitro or in vivo. For in vivo experiments, LNP were concentrated using centrifugal filters of the appropriate MWCO (20K for mRNA, 3.5K for siRNA LNP) at 2000 g for 20 min at 4 °C. Delivery of genetic cargo with LNPs was achieved by adding LNPs directly to cell culture media. Cargo included Firefly *Luciferase* mRNA (Trilink Biosciences, L-7202), siRNA for PU.1 (Horizon, M-041420/ orM-010537), and control nontargeting siRNA (Horizon, D-001810).

LNP Characterization: Size, polydispersity, and zeta potential were measured using a Malvern Zetasizer. Briefly, LNP solutions were diluted 100× in 1× PBS to a final volume of 1 mL in disposable polystyrene cuvettes to evaluate particle diameter and polydispersity. For zeta potential measurements, LNP solutions were instead diluted 100× in 0.1× PBS and measured in disposable folded capillary cells. Encapsulation efficiency was calculated using a Ribogreen Quant-iT entrapment assay (ThermoFisher, R11491) with fluorescence measured by a plate reader according to manufacturer's protocol and compared to a calibration curve of the encapsulated mRNA or siRNA cargo. LNP were diluted 100× in TE buffer with and without 2% Triton, and encapsulation efficiency was calculated as previously described.

$$EE\% = 1 - \frac{\text{Concentration}_{\text{Encapsulated}}}{\text{Concentration}_{\text{Free}}} \quad (1)$$

Mouse Experiments: All experiments with mice were performed in accordance with U.S. law and received ethical approval by the Committee for Animal Care of the Division of Comparative Medicine at Massachusetts Institute of Technology under protocol 0621-033-24. Mice were housed on a 12-h light-dark cycle at 24 °C, 45% relative humidity and food (Envigo, Teklad RMH 3000) and with water accessible ad libitum. Experiments were performed in male, two-month-old C57BL/6J (JAX, 000664) mice. Lipopolysaccharides (Millipore, L6529) were injected using a 1 mL syringe (BD, 309659) with a 26G needle (BD, 305110) at 10 mg kg^{-1} 1 d before behavioral experiments and perfusions. Intracisternal injection was performed with a 30G needle (BD, 305128) as described before.[61] The cap of the needle was cut 7 mm from the top, so that 2.5 mm of the needle protrudes beyond the opening. The needle and cut cap were attached to a Luer lock syringe (Hamilton, 81020). Immediately prior to injection, the back of the head was shaved with an electric razor in 2% isoflurane anesthetized mice. The area was then sterilized with three alternations of 70% ethanol and povidine. The needle insertion point (foramen magnum) was readily recognizable as a fold in the skin when the head was angled down. Ophthalmic ointment (Dechra, Puralube) was applied to both eyes. Neurodegeneration was assessed using the in-house CK-p25 mice[13] (and control littermate CK mice). In the CK-p25 mice, p25 expression was driven by the CaMKII-tTA (CK; JAX, 003010) promoter crossed to tetO-p25 mice (JAX, 005706). p25 expression was suppressed by rearing on 1 g kg^{-1} doxycycline diet (Bio-Rad, custom-made); p25 expression was induced by withdrawal of doxycycline and growth on regular diet. Open Field activity was recorded using a camera attached to the ceiling and analyzed automatically using EthoVision XT (Noldus) software. Open Field activity was averaged from two 10-min trials measuring the movement of the mouse in a custom-made plastic compartment measuring 40 × 40 cm. For *Luciferase* mRNA distribution, the mice were decapitated, and blood was collected from the neck, followed by collecting internal organs and dissecting the brain. The biopsies were then dounce-homogenized with a loose pestle (VWR, 62400-595) in Bright-Glo, spun at 15 000 rpm for 5 min. The supernatant was then transferred into a white 96-well plate (VWR, 354651) and measured for luminescence using an EnVision Multilabel Plate Reader (PerkinElmer, 2105-0010).

Reverse Transcriptase Quantitative Polymerase Chain Reaction (RT-qPCR): mRNA extraction was performed by use of the RNeasy Plus Mini Kit (Qiagen, 74134) and then converted into cDNA using the EcoDry RT PreMix reagent (Takara, 639542). cDNA was added to the SsoFast EvaGreen qPCR mastermix (Bio-Rad, 1725202) and primers were ordered from IDT, plated in Hard-Shell 96-well plates (Bio-Rad, Hsp9641), sealed (Bio-Rad, MSB1001), spun in a PCR plate spinner (Labnet, C1000) and, subsequently, gene expression was quantified using a qPCR detection system (Bio-Rad, CFX96) for 40 cycles. Relative gene expression changes were calculated using the $2^{-\Delta\Delta CT}$ method. Values were normalized to expression levels of *actb* (mouse) or *Actb* (human).

Immunohistology in Mice: Mice were deeply anesthetized with 5% isoflurane and intracardially perfused with 4 °C PBS, followed by dissection of the brain and/or peripheral organs, and subsequent drop-fixing in 4% paraformaldehyde overnight at 4 °C,[62] followed by sectioning into 40 µm coronal free-floating slices on a vibratome (Leica, VT1200S). Free-floating sections were transferred to blocking solution [5% normal donkey serum (Millipore, S30-M) and 0.3% Triton-X (Millipore, T8787)] and stained overnight in blocking solution with primary antibody at 4 °C. Secondary antibody was added in blocking solution for 30 min at room temperature, followed by three 10-min DPBS washes with 1 µg mL^{-1} Hoechst (ThermoFisher, H3570) added to the last wash. Finally, the glass coverslip was mounted using Fluoromount-G (VWR, 100502-406) and left to solidify overnight at room temperature. Confocal microscopy (Zeiss, LSM 880) was performed using a 20× Plan-Apochromat objective (Zeiss, 421452-9880-000). Livers were stained with hematoxylin and eosin Y (Tyr Scientific LLC) in the following sequence: sectioning, mounting on glass slide, dehydration in 100% xylene, 100% ethanol, 70% ethanol—followed by rehydration in deionized water and exposure to hematoxylin, bluing solution, 100% ethanol, eosin Y, 100% ethanol, and finally 100% xylene before coverslipping and imaging with a brightfield camera (Zeiss, LSM 900).

Statistical Analysis: All experiments were performed with at least three replicates, and each measurement was replicated at least three times.

Results are presented as mean ± SEM with individual data points also presented. Statistical analysis was performed using GraphPad Prism software. Unpaired Student's *t*-tests were performed when comparing two groups with $P \leq 0.05$ considered statistically significant.

Product	Source	Identifier
Anti-human CD11b-APC, 1:50	Miltenyi	130-113-231
Anti-human/mouse IBA1, 1:500	SYSY	234004
Anti-human NeuN-488	Millipore	MAB377X
Anti-human/mouse PU.1, 1:500	CST	2258S
Anti-human GLAST, 1:50	Miltenyi	130-095-822
Anti-human PU.1, 1:500	CST	2266S
Anti-mouse GFAP, 1:500	Abcam	Ab53554
Anti-mouse C1q, 1:500	Abcam	ab182451
CellTiter-Glo	Promega	G7570
Bright-Glo	Promega	E2610
Software		
ImageJ	NIH	https://imagej.net/Welcome
Prism	GraphPad	https://www.graphpad.com
EthoVisionXT	Noldus	https://www.noldus.com/ethovision-xt
Cyberduck	Open source	https://cyberduck.io/
RTqPCR primers		
TREM2-F	Human	ATGATGCGGGTCTCTACCAG
TREM2-R	Human	GGAACCAGAGATCTCCAGCA
IL1B-F	Human	GCATCCAGCTACGAATCTCC
IL1B-R	Human	TCGTTATCCCATGTGTCGAA
APOE-F	Human	CGCTTTTGGGATTACCTGCG
APOE-R	Human	GGGGTCAGTTGTTCCTCCAG
β ACTIN-F	Human	GGATGCAGAAGGAGATCACTG
β ACTIN-R	Human	CGATCCACACGGAGTACTTG
PU.1-F	Human	GCGTGCAAAATGGAAGGGTT
PU.1-R	Human	AGATCCGTGTCATAGGGCAC
TYROBP-F	Human	CCTGGCCGTGTACTTCCTG
TYROBP-R	Human	TCGCTGTAGACATCCGACCT
CCL2-F	Human	TCCCAAAGAAGCTGTGATCTTCA
CCL2-R	Human	TTTGCTTGTCCAGGTGGTCC
C1Q-F	Human	GCATCCAGTTGGAGTTGACA
C1Q-R	Human	GTCCTCGGTCACCATAGAGG
β actin-F	Mouse	CTCTGGCTCCTAGCACCATGAAGA
β actin-R	Mouse	GTAAAACGCAGCTCAGTAACAGTCCG
Pu.1-F	Mouse	GAGAAGCTGATGGCTTGGAG
Pu.1-R	Mouse	GGCGAATCTTTTTCTTGCTG
Il1b-F	Mouse	GAATCTATACCTGTCCTGTG
Il1b-R	Mouse	ATCTTGTTGAAGACAAACCG
Ccl2-F	Mouse	CACTCACCTGCTGCTACTCA
Ccl2-R	Mouse	GCTTGGTGACAAAAACTACAGC

Supporting Information

Supporting Information is available from the Wiley Online Library or from the author.

Acknowledgements

The authors would like to acknowledge the following individuals, agencies, and foundations for their kind support to this work: The JPB Foundation and the Picower Institute for Learning and Memory PIIF Engineering Collaboration Award (to L.-H.T. and R.S.L.), Robert and Renee Belfer Family, Eduardo Eurnekian, Lester A. Gimpelson, and Jay L. and Carroll Miller (to L.-H.T.). W.T.R. was supported by the Swiss National Science Foundation (Grants Nos. 177920 and 171909) and the Alzheimer's Association (Grant No. AARF-19-616816). J.L.A. was supported by a Koch Institute Graduate Fellowship.

Conflict of Interest

The authors declare no competing interests. For a list of entities with which R.L. is, or has been recently involved, compensated or uncompensated, see: https://www.dropbox.com/s/yc3xqb5s8s94v7x/Rev%20Langer%20COI.pdf?dl=0

Author Contributions

W.T.R. and J.L.A. contributed equally to this work. W.T.R., J.L.A., J.P., O.S.F., R.S.L., and L.-H.T. conceived of the study and wrote the manuscript. W.T.R., J.L.A, O.S.F., J.M.B., J.P., H.W., and M.M.H. performed the experiments and analyzed the results.

Data Availability Statement

The data that support the findings of this study are available from the corresponding author upon reasonable request.

Keywords

lipid nanoparticles, microglia, neurodegeneration, neuroinflammation, RNA delivery

Received: September 7, 2023
Revised: November 22, 2023
Published online: December 8, 2023

[1] W.-W. Chen, X. Zhang, W.-J. Huang, *Mol. Med. Rep.* **2016**, *13*, 3391.
[2] H. S. Kwon, S.-H. Koh, *Transl. Neurodegener.* **2020**, *9*, 42.
[3] S. Amor, F. Puentes, D. Baker, P. Van Der Valk, *Immunology* **2010**, *129*, 154.
[4] T. P. J. Knowles, M. Vendruscolo, C. M. Dobson, *Nat. Rev. Mol. Cell Biol.* **2014**, *15*, 384.
[5] B. E. Deverman, B. M. Ravina, K. S. Bankiewicz, S. M. Paul, D. W. Y. Sah, *Nat. Rev. Drug Discovery* **2018**, *17*, 641.
[6] G. Day, N. Scarmeas, R. Dubinsky, K. Coerver, A. Mostacero, B. West, S. Wessels, M. Armstrong, *Neurolog* **2022**, *15*, 619.
[7] S. Hickman, S. Izzy, P. Sen, L. Morsett, J. El Khoury, *Nat. Neurosci.* **2018**, *21*, 1359.
[8] F. L. Heppner, R. M. Ransohoff, B. Becher, *Nat. Rev. Neurosci.* **2015**, *16*, 358.
[9] J. Penney, W. T. Ralvenius, L.-H. Tsai, *Mol. Psychiatry* **2020**, *25*, 148.
[10] A. M. Smith, H. M. Gibbons, R. L. Oldfield, P. M. Bergin, E. W. Mee, R. L. M. Faull, M. Dragunow, *Glia* **2013**, *61*, 929.
[11] A. A. Pimenova, M. Herbinet, I. Gupta, S. I. Machlovi, K. R. Bowles, E. Marcora, A. M. Goate, *Neurobiol. Dis.* **2021**, *148*, 105217.

[12] E. Gjoneska, A. R. Pfenning, H. Mathys, G. Quon, A. Kundaje, L.-H. Tsai, M. Kellis, *Nature* **2015**, *518*, 365.
[13] K.-L. Huang, E. Marcora, A. A. Pimenova, A. F. Di Narzo, M. Kapoor, S. C. Jin, O. Harari, S. Bertelsen, B. P. Fairfax, J. Czajkowski, V. Chouraki, B. Grenier-Boley, C. Bellenguez, Y. Deming, A. Mckenzie, T. Raj, A. E. Renton, J. Budde, A. Smith, A. Fitzpatrick, J. C. Bis, A. Destefano, H. H. H. Adams, M. A. Ikram, S. Van Der Lee, J. L. Del-Aguila, M. V. Fernandez, L. Ibañez, R. Sims, V. Escott-Price, et al., *Nat. Neurosci.* **2017**, *20*, 1052.
[14] H. Cao, X. Zhou, Y. Chen, F. C. F. Ip, Y. Chen, N. C. H. Lai, R. M. N. Lo, E. P. S. Tong, V. C. T. Mok, T. C. Y. Kwok, A. N. Initiative, A. K. Y. Fu, N. Y. Ip, *J. Alzheimer's Dis.* **2022**, *86*, 1861.
[15] N. M. Dräger, S. M. Sattler, C. T.-L. Huang, O. M. Teter, K. Leng, S. H. Hashemi, J. Hong, G. Aviles, C. D. Clelland, L. Zhan, J. C. Udeochu, L. Kodama, A. B. Singleton, M. A. Nalls, J. Ichida, M. E. Ward, F. Faghri, L. Gan, M. Kampmann, *Nat. Neurosci.* **2022**, *25*, 1149.
[16] J. Rustenhoven, A. M. Smith, L. C. Smyth, D. Jansson, E. L. Scotter, M. E. V. Swanson, M. Aalderink, N. Coppieters, P. Narayan, R. Handley, C. Overall, T. I. H. Park, P. Schweder, P. Heppner, M. A. Curtis, R. L. M. Faull, M. Dragunow, *Mol. Neurodegener.* **2018**, *13*, 44.
[17] W. T. Ralvenius, A. E. Mungenast, H. Woolf, M. M. Huston, T. Z. Gillingham, S. K. Godin, J. Penney, H. P. Cam, F. Gao, C. G. Fernandez, B. Czako, Y. Lightfoot, W. J. Ray, A. Beckmann, A. M. Goate, E. Marcora, C. Romero-Molina, P. Ayata, A. Schaefer, E. Gjoneska, L.-H. Tsai, *J. Exp. Med.* **2023**, *220*, e20222105.
[18] W. M. Pardridge, *Front. Aging Neurosci.* **2020**, *11*, 373.
[19] S. F. Dowdy, *Nat. Biotechnol.* **2017**, *35*, 222.
[20] H. Yin, R. L. Kanasty, A. A. Eltoukhy, A. J. Vegas, J. R. Dorkin, D. G. Anderson, *Nat. Rev. Genet.* **2014**, *15*, 541.
[21] R. Kanasty, J. R. Dorkin, A. Vegas, D. Anderson, *Nat. Mater.* **2013**, *12*, 967.
[22] K. A. Whitehead, R. Langer, D. G. Anderson, *Nat. Rev. Drug Discovery* **2009**, *8*, 129.
[23] J. L. Andresen, O. S. Fenton, *MRS Bull.* **2021**, *46*, 832.
[24] F. P. Polack, S. J. Thomas, N. Kitchin, J. Absalon, A. Gurtman, S. Lockhart, J. L. Perez, G. Pérez Marc, E. D. Moreira, C. Zerbini, R. Bailey, K. A. Swanson, S. Roychoudhury, K. Koury, P. Li, W. V. Kalina, D. Cooper, R. W. Frenck, L. L. Hammitt, Ö. Türeci, H. Nell, A. Schaefer, S. Ünal, D. B. Tresnan, S. Mather, P. R. Dormitzer, U. Sahin, K. U. Jansen, W. C. Gruber, *N. Engl. J. Med.* **2020**, *383*, 2603.
[25] L. R. Baden, H. M. El Sahly, B. Essink, K. Kotloff, S. Frey, R. Novak, D. Diemert, S. A. Spector, N. Rouphael, C. B. Creech, J. Mcgettigan, S. Khetan, N. Segall, J. Solis, A. Brosz, C. Fierro, H. Schwartz, K. Neuzil, L. Corey, P. Gilbert, H. Janes, D. Follmann, M. Marovich, J. Mascola, L. Polakowski, J. Ledgerwood, B. S. Graham, H. Bennett, R. Pajon, C. Knightly, et al., *N. Engl. J. Med.* **2021**, *384*, 403.
[26] C. Lorenzer, M. Dirin, A.-M. Winkler, V. Baumann, J. Winkler, *J. Controlled Release* **2015**, *203*, 1.
[27] Y.-N. Zhang, W. Poon, A. J. Tavares, I. D. Mcgilvray, W. C. W. Chan, *J. Controlled Release* **2016**, *240*, 332.
[28] Y. Dong, K. T. Love, J. R. Dorkin, S. Sirirungruang, Y. Zhang, D. Chen, R. L. Bogorad, H. Yin, Y. Chen, A. J. Vegas, C. A. Alabi, G. Sahay, K. T. Olejnik, W. Wang, A. Schroeder, A. K. R. Lytton-Jean, D. J. Siegwart, A. Akinc, C. Barnes, S. A. Barros, M. Carioto, K. Fitzgerald, J. Hettinger, V. Kumar, T. I. Novobrantseva, J. Qin, W. Querbes, V. Koteliansky, R. Langer, D. G. Anderson, *Proc. Natl. Acad. Sci. USA* **2014**, *111*, 3955.
[29] D. Lalka, R. K. Griffith, C. L. Cronenberger, *J. Clin. Pharmacol.* **1993**, *33*, 657.
[30] H. Gao, K. Matyjaszewski, *J. Am. Chem. Soc.* **2007**, *129*, 6633.
[31] F. Ma, L. Yang, Z. Sun, J. Chen, X. Rui, Z. Glass, Q. Xu, *Sci. Adv.* **2020**, *6*, eabb4429.
[32] H. Tanaka, T. Nakatani, T. Furihata, K. Tange, Y. Nakai, H. Yoshioka, H. Harashima, H. Akita, *Mol. Pharm.* **2018**, *15*, 2060.
[33] B. Choi, M.-H. Ahn, S. Hong, E. E. Barcelon, J. Sangshetti, R. B. Arote, S. J. Lee, *RSC Adv.* **2021**, *11*, 36792.
[34] H. K. Dhaliwal, Y. Fan, J. Kim, M. M. Amiji, *Mol. Pharm.* **2020**, *17*, 1996.
[35] S. Guo, F. Cázarez-Márquez, H. Jiao, E. Foppen, N. L. Korpel, A. E. Grootemaat, N. Liv, Y. Gao, N. Van Der Wel, B. Zhou, G. Nie, C.-X. Yi, *ACS Appl. Mater. Interfaces* **2022**, *14*, 5066.
[36] Z. R. Cohen, S. Ramishetti, N. Peshes-Yaloz, M. Goldsmith, A. Wohl, Z. Zibly, D. Peer, *ACS Nano* **2015**, *9*, 1581.
[37] A. E. Mungenast, S. Siegert, L.-H. Tsai, *Mol. Cell. Neurosci.* **2016**, *73*, 13.
[38] J. Muffat, Y. Li, B. Yuan, M. Mitalipova, A. Omer, S. Corcoran, G. Bakiasi, L.-H. Tsai, P. Aubourg, R. M. Ransohoff, R. Jaenisch, *Nat. Med.* **2016**, *22*, 1358.
[39] A. Mcquade, M. Coburn, C. H. Tu, J. Hasselmann, H. Davtyan, M. Blurton-Jones, *Mol. Neurodegener.* **2018**, *13*, 67.
[40] G. Sienski, P. Narayan, J. M. Bonner, N. Kory, S. Boland, A. A. Arczewska, W. T. Ralvenius, L. Akay, E. Lockshin, L. He, B. Milo, A. Graziosi, V. Baru, C. A. Lewis, M. Kellis, D. M. Sabatini, L.-H. Tsai, S. Lindquist, *Sci. Transl. Med.* **2021**, *13*, eaaz4564.
[41] H. Xue, P. Guo, W.-C. Wen, H. Wong, *Curr. Pharm. Des.* **2015**, *21*, 3140.
[42] O. S. Fenton, K. N. Olafson, P. S. Pillai, M. J. Mitchell, R. Langer, *Adv. Mater.* **2018**, *30*, 1705328.
[43] D. Chen, K. T. Love, Y. Chen, A. A. Eltoukhy, C. Kastrup, G. Sahay, A. Jeon, Y. Dong, K. A. Whitehead, D. G. Anderson, *J. Am. Chem. Soc.* **2012**, *134*, 6948.
[44] K. J. Kauffman, J. R. Dorkin, J. H. Yang, M. W. Heartlein, F. Derosa, F. F. Mir, O. S. Fenton, D. G. Anderson, *Nano Lett.* **2015**, *15*, 7300.
[45] E. Álvarez-Benedicto, L. Farbiak, M. Márquez Ramírez, X. Wang, L. T. Johnson, O. Mian, E. D. Guerrero, D. J. Siegwart, *Biomater. Sci.* **2022**, *10*, 549.
[46] L. Yang, F. Ma, F. Liu, J. Chen, X. Zhao, Q. Xu, *Mol. Ther.–Nucleic Acids* **2020**, *19*, 1357.
[47] M. J. Carrasco, S. Alishetty, M.-G. Alameh, H. Said, L. Wright, M. Paige, O. Soliman, D. Weissman, T. E. Cleveland, A. Grishaev, M. D. Buschmann, *Commun. Biol.* **2021**, *4*, 956.
[48] M. P. Lokugamage, Z. Gan, C. Zurla, J. Levin, F. Z. Islam, S. Kalathoor, M. Sato, C. D. Sago, P. J. Santangelo, J. E. Dahlman, *Adv. Mater.* **2020**, *32*, 1904905.
[49] K. Karikó, H. Muramatsu, F. A. Welsh, J. Ludwig, H. Kato, S. Akira, D. Weissman, *Mol. Ther.* **2008**, *16*, 1833.
[50] P. P. G. Guimaraes, R. Zhang, R. Spektor, M. Tan, A. Chung, M. M. Billingsley, R. El-Mayta, R. S. Riley, L. Wang, J. M. Wilson, M. J. Mitchell, *J. Controlled Release* **2019**, *316*, 404.
[51] K. Paunovska, C. D. Sago, C. M. Monaco, W. H. Hudson, M. G. Castro, T. G. Rudoltz, S. Kalathoor, D. A. Vanover, P. J. Santangelo, R. Ahmed, A. V. Bryksin, J. E. Dahlman, *Nano Lett.* **2018**, *18*, 2148.
[52] L. Miao, J. Lin, Y. Huang, L. Li, D. Delcassian, Y. Ge, Y. Shi, D. G. Anderson, *Nat. Commun.* **2020**, *11*, 2424.
[53] H. Peluffo, U. Unzueta, M. L. Negro-Demontel, Z. Xu, E. Váquez, N. Ferrer-Miralles, A. Villaverde, *Biotechnol. Adv.* **2015**, *33*, 277.
[54] D. Rosenblum, A. Gutkin, R. Kedmi, S. Ramishetti, N. Veiga, A. M. Jacobi, M. S. Schubert, D. Friedmann-Morvinski, Z. R. Cohen, M. A. Behlke, J. Lieberman, D. Peer, *Sci. Adv.* **2020**, *6*, eabc9450.
[55] R. L. Rungta, H. B. Choi, P. J. Lin, R. W. Ko, D. Ashby, J. Nair, M. Manoharan, P. R. Cullis, B. A. Macvicar, *Mol. Ther.–Nucleic Acids* **2013**, *2*, 136,
[56] J. C. Cruz, H.-C. Tseng, J. A. Goldman, H. Shih, L.-H. Tsai, *Neuron* **2003**, *40*, 471.

[57] J. Yu, L. Liu, H. Zhang, Y. Wu, H. Pei, L. Ma, A. Xiong, C. Xie, *RSC Adv.* **2018**, *8*, 33338.
[58] H. Mathys, C. Adaikkan, F. Gao, J. Young, E. Manet, M. Hemberg, P. De Jager, R. Ransohoff, A. Regev, L. Tsai, *Cell Rep.* **2017**, *21*, 366.
[59] Y.-T. Lin, J. Seo, F. Gao, H. M. Feldman, H.-L. Wen, J. Penney, H. P. Cam, E. Gjoneska, W. K. Raja, J. Cheng, R. Rueda, O. Kritskiy, F. Abdurrob, Z. Peng, B. Milo, C. J. Yu, S. Elmsaouri, D. Dey, T. Ko, B. A. Yankner, L.-H. Tsai, *Neuron* **2018**, *98*, 1141.
[60] M. Munde, S. Wang, A. Kumar, C. E. Stephens, A. A. Farahat, D. W. Boykin, W. D. Wilson, G. M. K. Poon, *Nucleic Acids Res.* **2014**, *421*.
[61] O. S. Fenton, K. J. Kauffman, R. L. Mcclellan, J. C. Kaczmarek, M. D. Zeng, J. L. Andresen, L. H. Rhym, M. W. Heartlein, F. Derosa, D. G. Anderson, *Angew. Chem., Int. Ed.* **2018**, *57*, 13582.
[62] S. C. Hofer, W. T. Ralvenius, M. S. Gachet, J.-M. Fritschy, H. U. Zeilhofer, J. Gertsch, *Neuropharmacology* **2015**, *98*, 78.